Supporting Information

Zn(II)-based coordination polymer: An emissive signaling platform for the recognition of an explosive and a pesticide in an aqueous system

Trivender kumar,[a] M. Venkateswarulu,[a] Bidisa Das,[b] Aditi Halder[a]* and Rik Rani Koner[c]*

[a]*School of Basic Sciences, Indian Institute of Technology Mandi, Mandi-175001, H.P., India.*

[b]*Technical Research Center (TRC), Indian Association for the Cultivation of Science (IACS), 2A & 2B Raja S C Mullick Road. Jadavpur, Kolkata-700032, India.*

[c]*School of Engineering, Indian Institute of Technology Mandi, Mandi-175001, H.P., India.*

Table of Contents

1. Materials and general methods:

All the chemicals were purchased from TCI, Alfa Aesar and Sigma Aldrich and were used without further purification. HPLC grade solvent was used for the spectral studies. The analytes nitrobenzene (NB), 1,4-dinitrobenzene (1,4-DNB), 2,4,6-trinitrotoluene (TNT), paranitrophenol (PNP), 2,4-dinitrophenol (2,4-DNP) 2,4,6-trinitrophenol (TNP), triethylamine (TEA), ethylenediamine (EDA), aniline, carbaryl, nicotine, ethion and paranitroaniline (PNA) were purchased from Sigma Aldrich. 2,6-naphthalene dicarboxylic acid (NDC) and 2,6-dichloro-4-nitroaniline (2,6-DCNA) was obtained from TCI and used as received. Single-crystals X-ray diffraction studies were performed on Supernova X-ray diffractometer of Agilent Technologies. Powder X-ray diffraction (PXRD) data were collected on Rigaku Smart Lab, X-ray diffractometer using Cu-Kα radiation ($\lambda = 1.54184$ Å) at 45 kV and 100 mA at room temperature. The thermogravimetric analysis (TGA) was carried out using PerkinElmer, Pyris 1 TGA (Thermogravimetric Analyzer) in N_2 atmosphere at a heating rate of 10 °C/min from room temperature to 800 °C. Gas adsorption measurements was performed using Autosorb iQ3 gas sorption analyzer, Quantachrome Instruments. Absorption spectra were recorded on SHIMADZU UV-2450 Spectrophotometer. The fluorescence spectra were recorded on Cary Eclipse Fluorescence Spectrophotometer of Agilent Technologies.

Caution! TNP and TNT are highly explosive and should be handled carefully in small amounts as dilute solutions with safety measures to avoid explosion.

2. Synthesis of probe Zn-CP:

In a 15ml glass vial, $Zn(NO_3)_2 \cdot 6H_2O$ (13.68 mg, 0.046 mmol), 2,6 naphthalene dicarboxylic acid (10 mg, 0.046 mmol), and 2-methyl imidazole (3.77 mg, 0.046 mmol) were dissolved in DMF/ ethanol mixture (2:1). Then the glass vial was tightened and kept at 80 °C for 2 days. The transparent colorless cube shaped crystals were obtained. After cooling to room temperature, the colorless crystals were isolated by filtration and washed with DMF/Ethanol (2:1) mixture. Yield: 73 % (based on Zn).

3. Fluorescence study:

The aqueous dispersion of Zn-CP was prepared by adding 2 mg of Zn-CP into 4 ml of water, then it was ultrasonicated for 45 min. After that, 2 mL of this solution was further diluted to 50 mL by adding water to it and kept it for two days to stabilize the suspension for spectral studies. All the fluorescence studies were executed in a 3 mL quartz cuvette of 1 cm path length. The fluorescence spectra were recorded after the incremental addition of freshly prepared (1mM) stock solutions of all analytes. For all measurements the dispersed solution was excited at 325 nm and corresponding emission intensity was monitored at 369 nm. Each measurement was repeated by three times.

4. Single-crystal X-ray diffraction analysis (SCXRD):

The crystal suitable for single crystal X-ray structural studies of Zn-CP was synthesized by solvothermal method and performed on Supernova X-ray diffractometer system of Agilent Technologies using graphite-monochromatic Cu-Kα radiation (λ = 1.54184Å) at 150 K. The data was collected by the standard 'phi-omega scan techniques in which the crystal is mounted on the 4-circle kappa goniometer which gradually rotated while being bombarded with X-rays, producing a diffraction pattern of spaced spots called reflections. CrysAlisPro Software (online version) was used for data collection and CrysAlisPro Software (offline version) used for data reduction.[1] The SCXRD data revealed that the Zn-CP crystalized in triclinic crystal system with the space group

P-1. The structure was solved by direct methods using olex2 and refined by full matrix least-squares on F^2 with the SHELXL-97 program.[2,3]

Table S1. Single-crystal data and structure refinement parameters of Zn-CP.

Compound	Zn-CP
Empirical formula	$C_{37}H_{39}N_5O_{11}Zn_2$
Formula weight	860.47
Temperature (K)	150(10)
Crystal system	Triclinic
Space group	P-1
a (Å)	11.7332(9)
b (Å)	13.0684(8)
c (Å)	13.1512(7)
α (deg.)	84.610(5)
β (deg.)	88.522(5)
γ (deg.)	69.276(7)
Volume (Å^3)	1877.7(2)
Z	2
ρcalc (g/cm^3)	1.522
μ (mm^{-1})	2.145
F(000)	888.0
Crystal size (mm^3)	0.108 × 0.094 × 0.069
Radiation	Cu-Kα (λ = 1.54184 Å)
2θ range for data collection (deg.)	6.76 to 133.9
Index ranges	$-12 \leq h \leq 13$, $-14 \leq k \leq 15$, $-14 \leq l \leq 15$
Reflections collected	11191
Independent reflections	6379 [R_{int} = 0.1186, R_{sigma} = 0.1099]
Data/restraints/parameters	6379/0/453
Goodness-of-fit on F^2	1.041

Final R indexes [I>=2σ (I)]	$R_1 = 0.0839$, $wR_2 = 0.2212$
Final R indexes [all data]	$R_1 = 0.1091$, $wR_2 = 0.2481$
Largest diff. peak/hole (e Å^{-3})	2.00/-1.20

Table S2: Selected bond length (Å) observed in Zn-CP.

Bond	Distance (Å)	Bond	Distance (Å)
Zn1-O2	2.046(4)	Zn2-O1	2.069(4)
Zn1-O3	2.067(4)	Zn2-O4	2.011(4)
Zn1-O6	2.056(4)	Zn2-O5	2.051(4)
Zn1-O8	2.061(4)	Zn2-O7	2.041(4)
Zn1-N1	2.010(4)	Zn2-O9	1.985(4)

Table S3: Selected bond angle (degree) observed in Zn-CP.

Bond	Angle (deg.)	Bond	Angle (deg.)
O2 Zn1 O6	158.03(17)	O5 Zn2 O1	157.42(17)
O2 Zn1 O3	87.42(18)	O9 Zn2 O5	100.30(16)
O2 Zn1 O8	85.64(18)	O9 Zn2 O1	102.24(17)
O6 Zn1 O3	88.14(17)	O9 Zn2 O4	99.49(16)
O6 Zn1 O8	88.69(17)	O9 Zn2 O7	97.63(15)
O8 Zn1 O3	153.14(17)	O4 Zn2 O5	89.38(17)
N1 Zn1 O3	105.49(17)	O4 Zn2 O1	88.35(19)
N1 Zn1 O2	105.38(18)	O4 Zn2 O7	162.88(17)
N1 Zn1 O6	96.54(17)	O7 Zn2 O1	87.87(18)
N1 Zn1 O8	101.37(17)	O7 Zn2 O5	87.74(17)
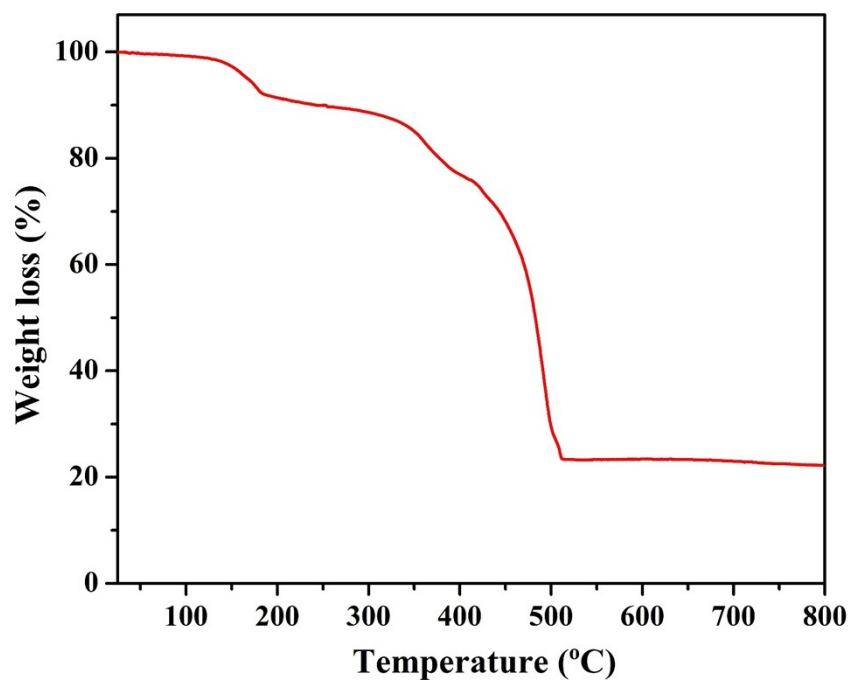
Figure S1. Thermogravimetric analysis of Zn-CP in N_2 atmosphere.
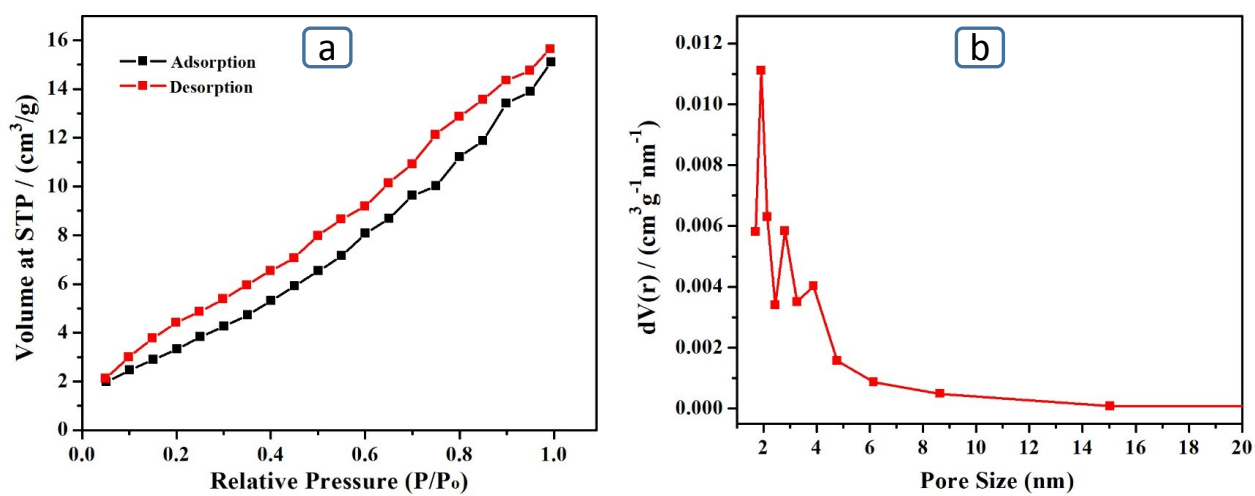
Figure S2. (a) N_2 sorption isotherm of Zn-CP at 77 K. (b) Pore size distribution curve of Zn-CP.
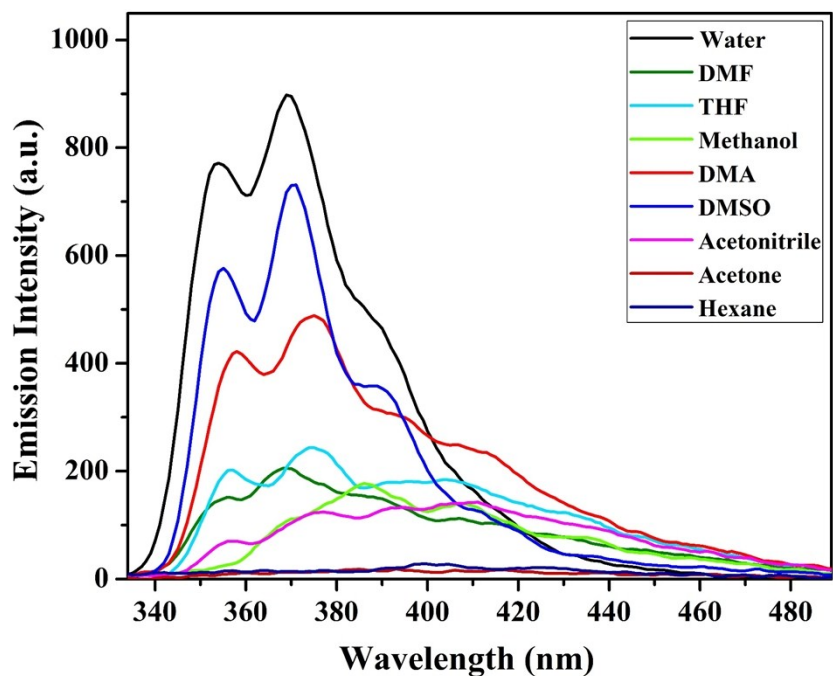
Figure S3. Effect of different solvent in the emission spectrum of Zn-CP. (λ_{ex} = 325 nm, λ_{em} = 369 nm).
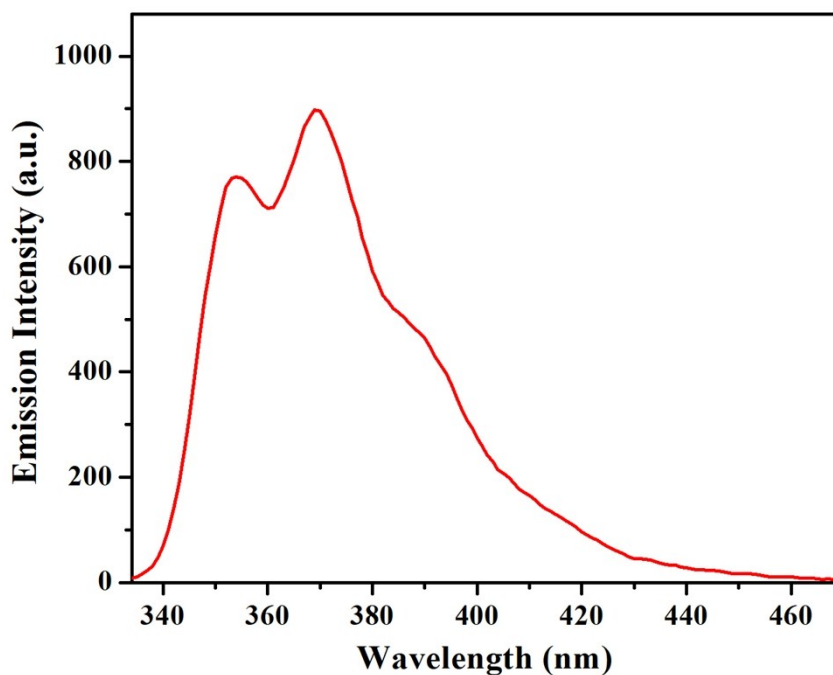
Figure S4. Emission spectrum of Zn-CP dispersed in water (λ_{ex} = 325 nm, λ_{em} = 369 nm).
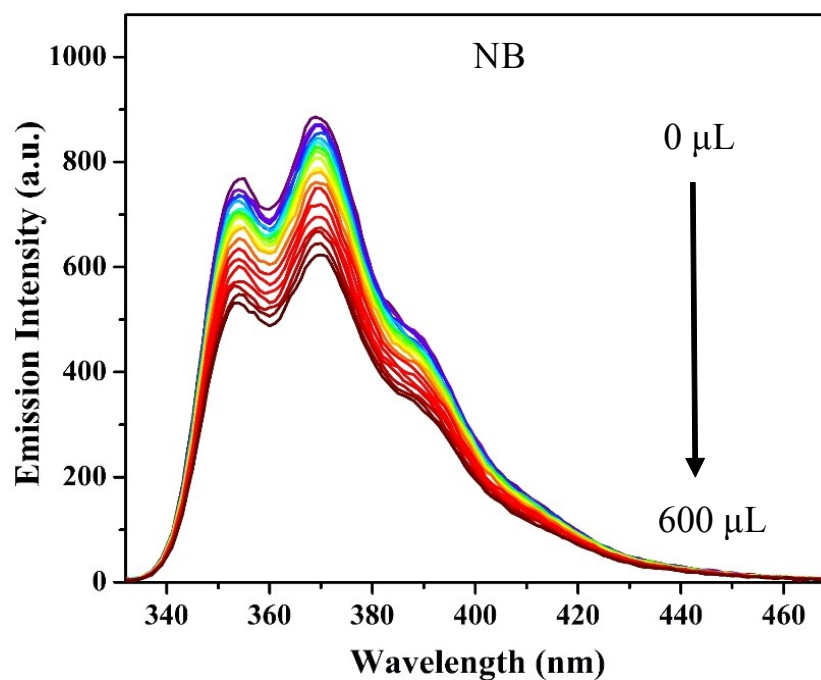
Figure S5. Reduction in emission intensity of Zn-CP dispersed in water upon incremental addition of NB solution (1mM) (λ_{ex} = 325 nm).
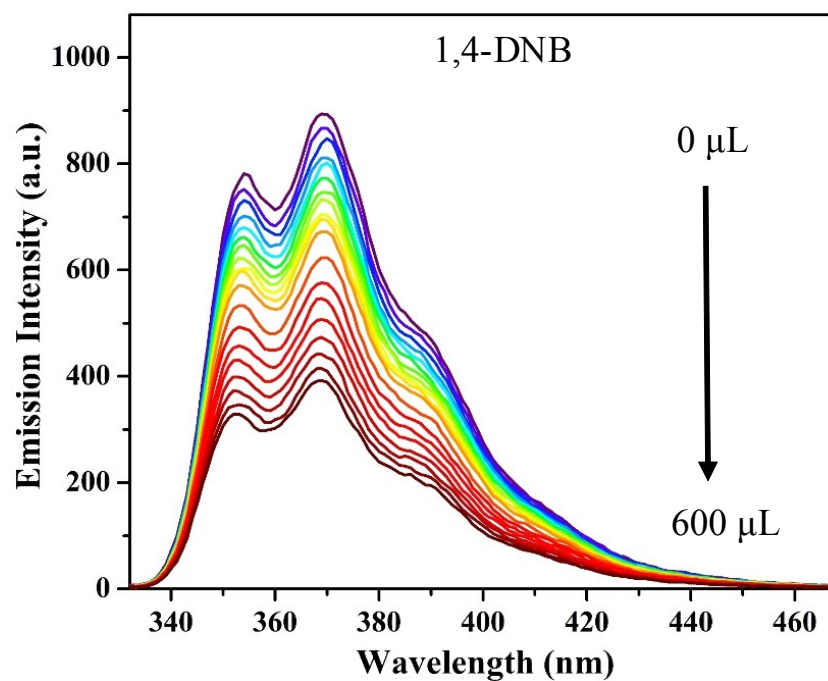
Figure S6. Reduction in emission intensity of Zn-CP dispersed in water upon incremental addition of 1,4-DNB solution (1mM) (λ_{ex} = 325 nm).
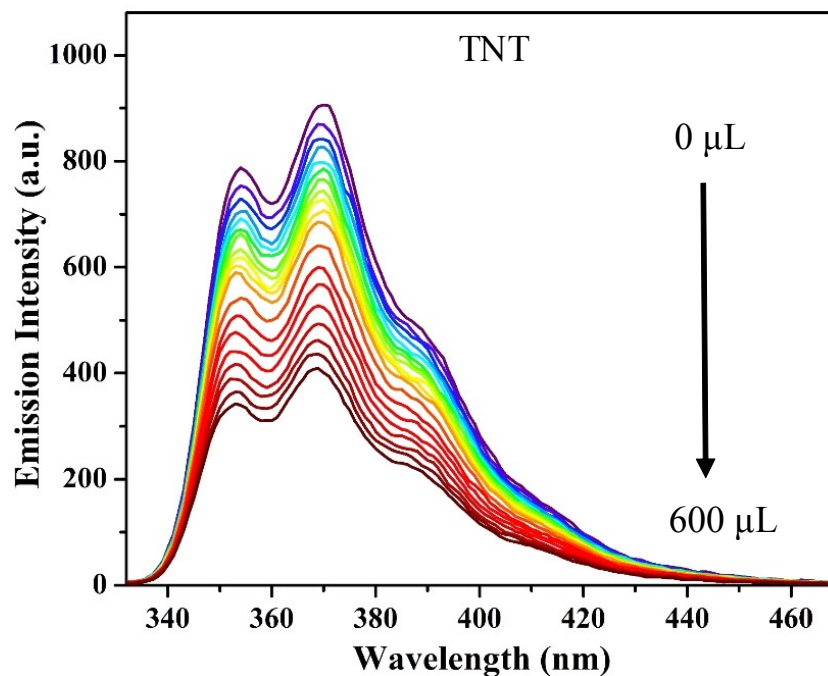
Figure S7. Reduction in emission intensity of Zn-CP dispersed in water upon incremental addition of TNT solution (1mM) (λ_{ex} = 325 nm).
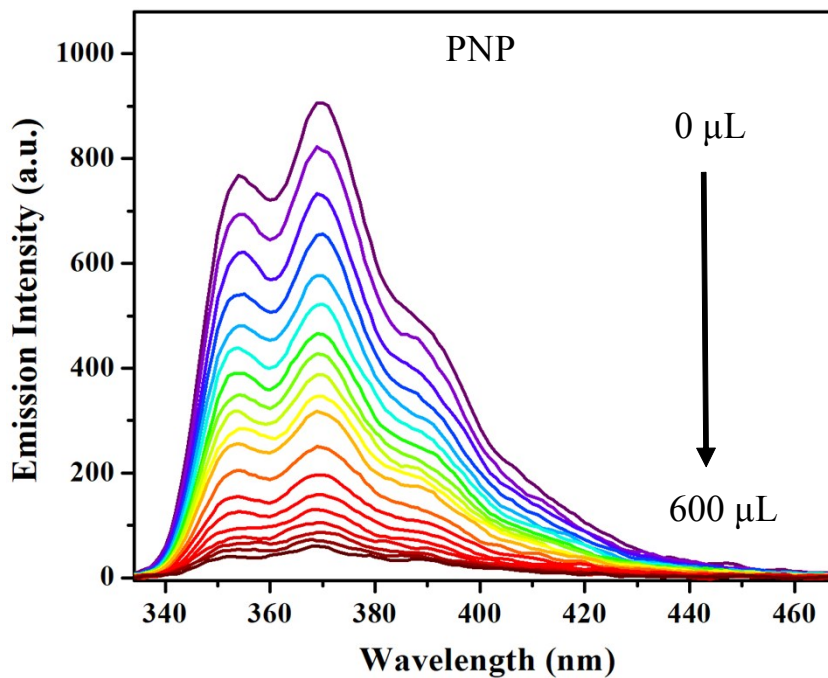
Figure S8. Reduction in emission intensity of Zn-CP dispersed in water upon incremental addition of PNP solution (1mM) (λ_{ex} = 325 nm).
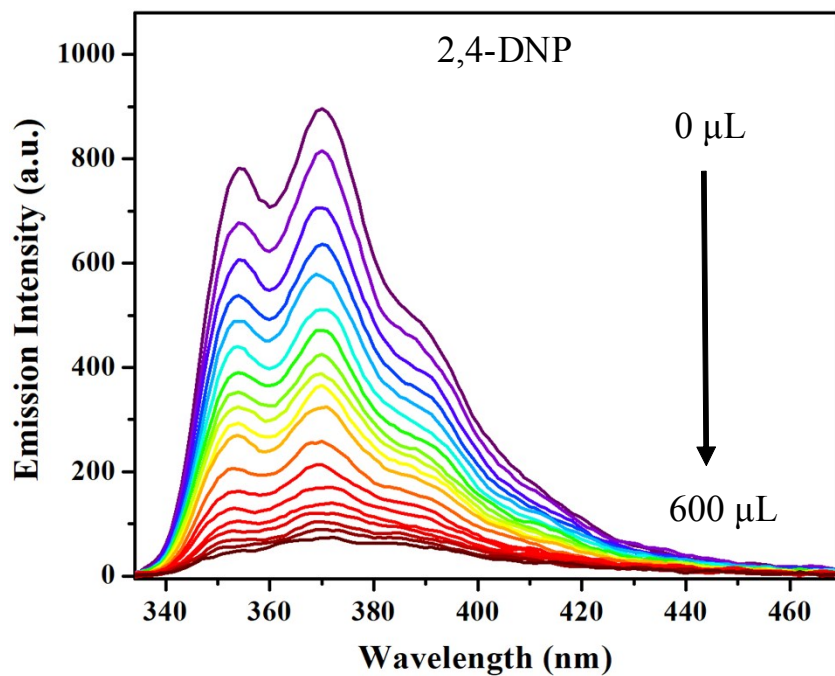
Figure S9. Reduction in emission intensity of Zn-CP dispersed in water upon incremental addition of 2,4-DNP solution (1mM) (λ_{ex} = 325 nm).
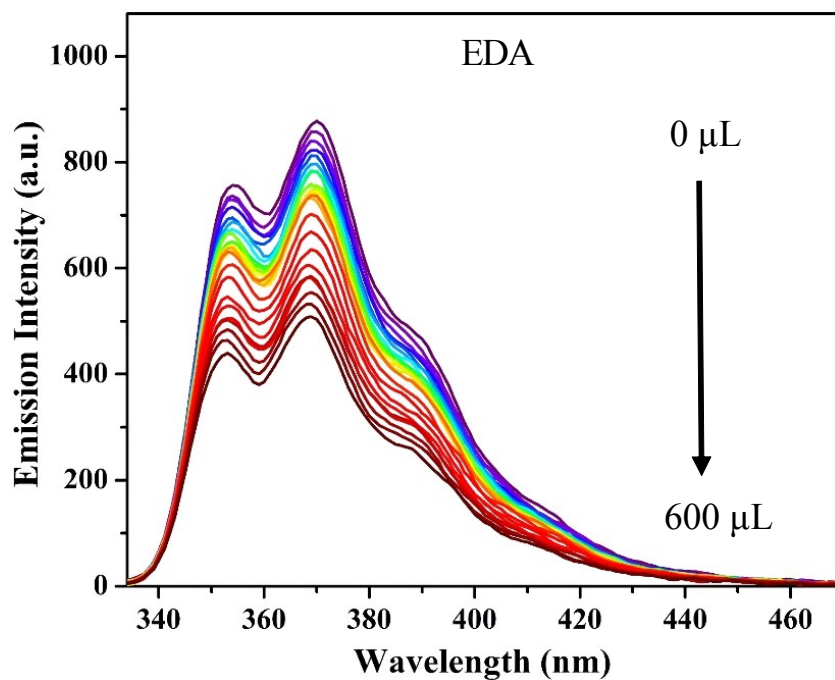
Figure S10. Reduction in emission intensity of Zn-CP dispersed in water upon incremental addition of EDA solution (1mM) (λ_{ex} = 325 nm).
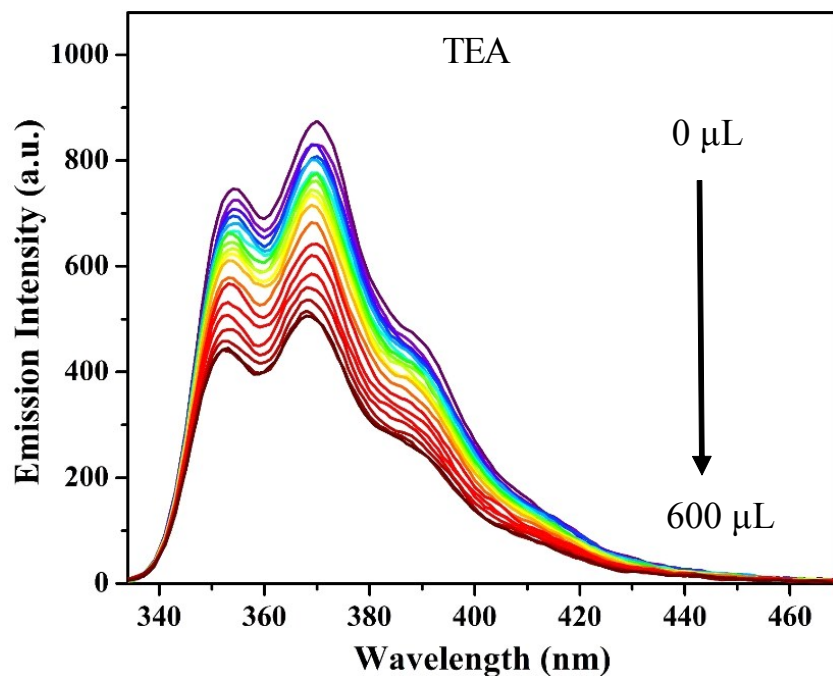
Figure S11. Reduction in emission intensity of Zn-CP dispersed in water upon incremental addition of TEA solution (1mM) (λ_{ex} = 325 nm).
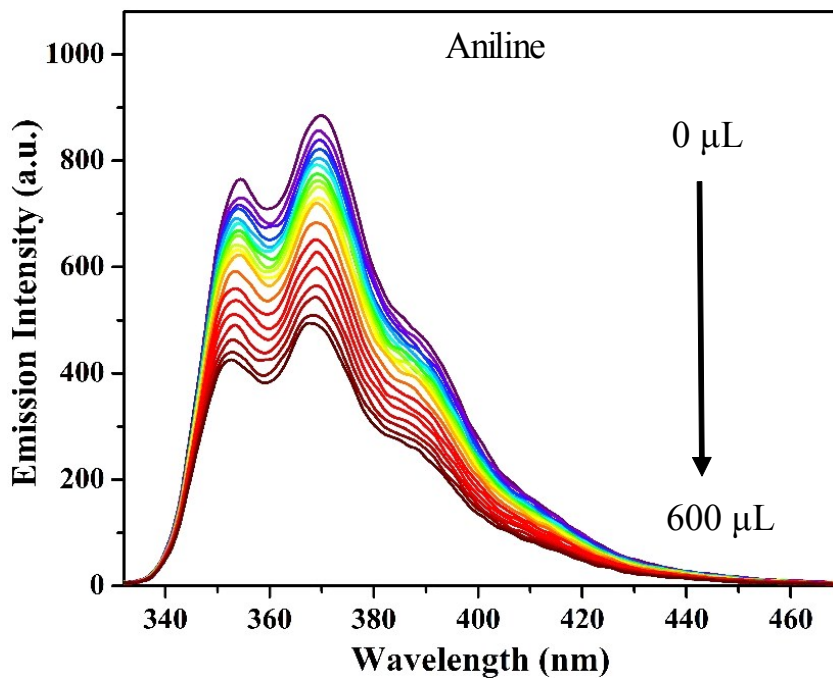
Figure S12. Reduction in emission intensity of Zn-CP dispersed in water upon incremental addition of aniline solution (1mM) (λ_{ex} = 325 nm).
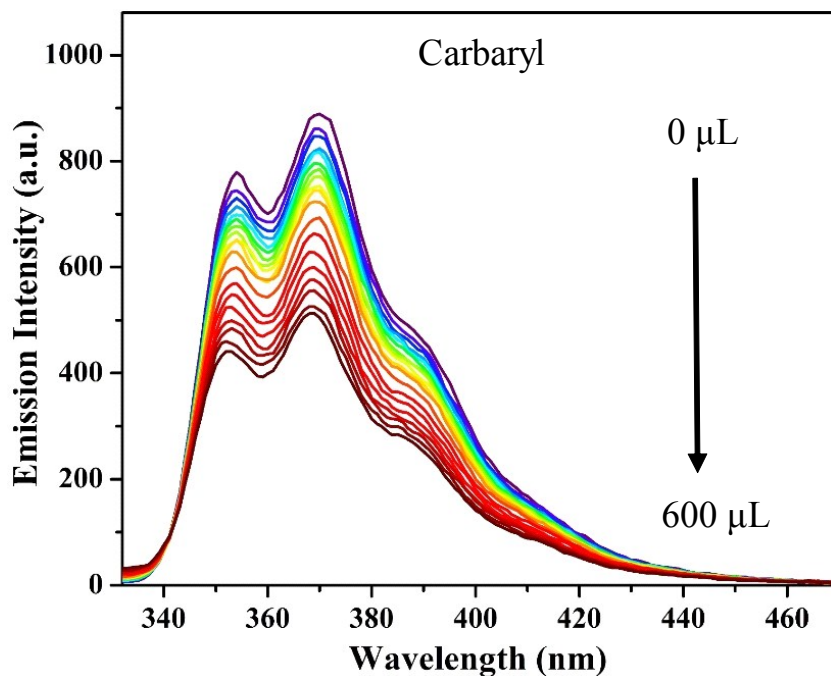
Figure S13. Reduction in emission intensity of Zn-CP dispersed in water upon incremental addition of carbaryl solution (1mM) (λ_{ex} = 325 nm).
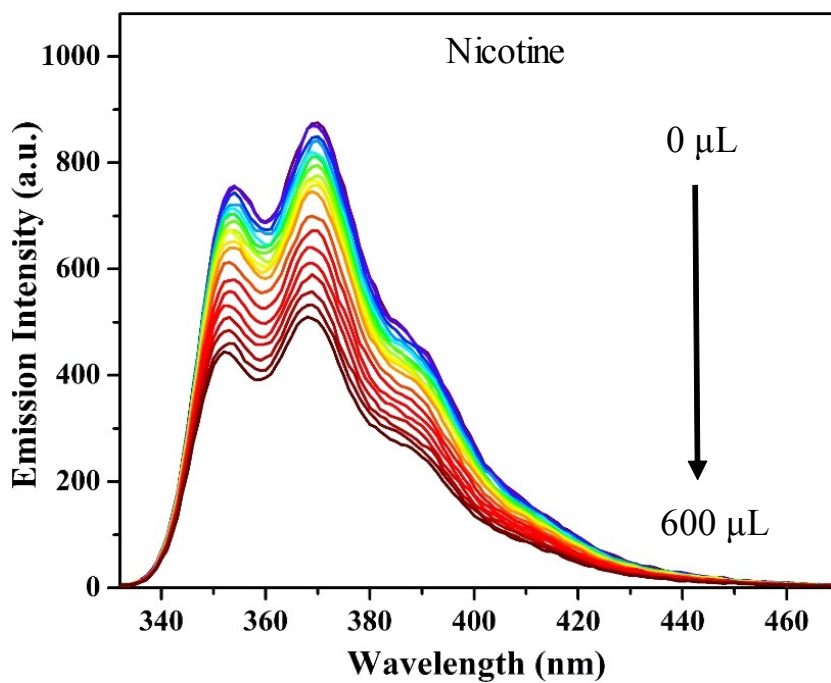
Figure S14. Reduction in emission intensity of Zn-CP dispersed in water upon incremental addition of nicotine solution (1mM) (λ_{ex} = 325 nm).
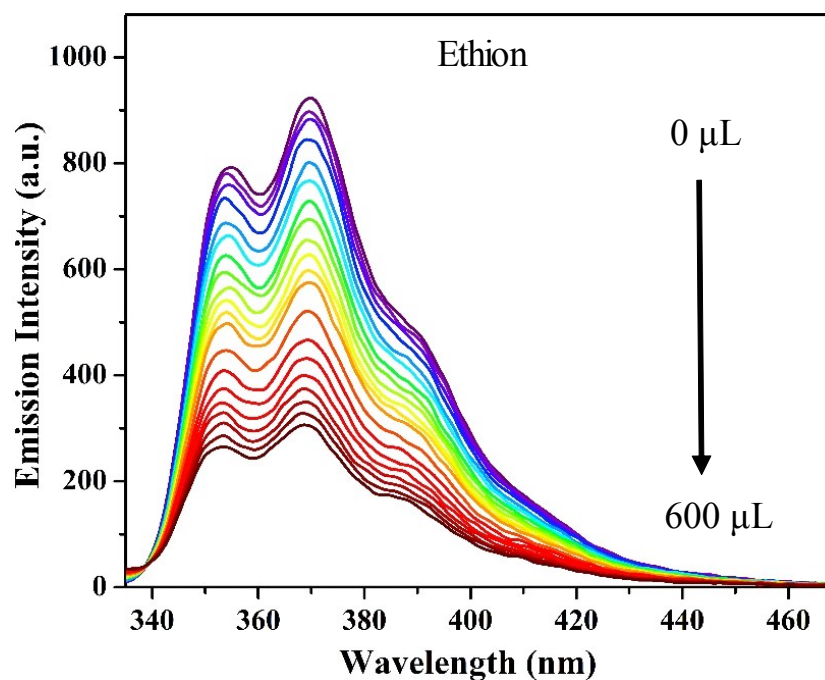
Figure S15. Reduction in emission intensity of Zn-CP dispersed in water upon incremental addition of ethion solution (1mM) (λ_{ex} = 325 nm).
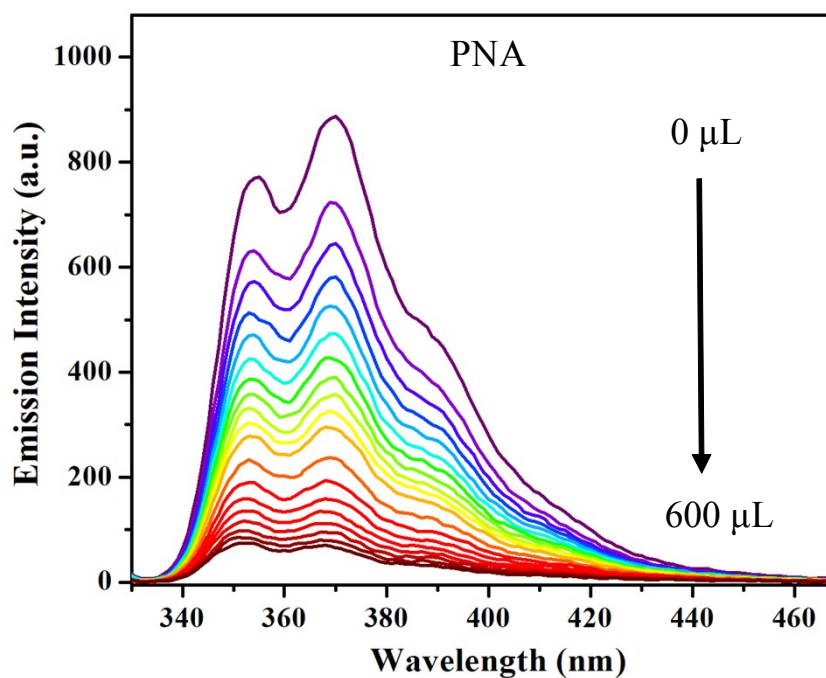
Figure S16. Reduction in emission intensity of Zn-CP dispersed in water upon incremental addition of PNA solution (1mM) (λ_{ex} = 325 nm).
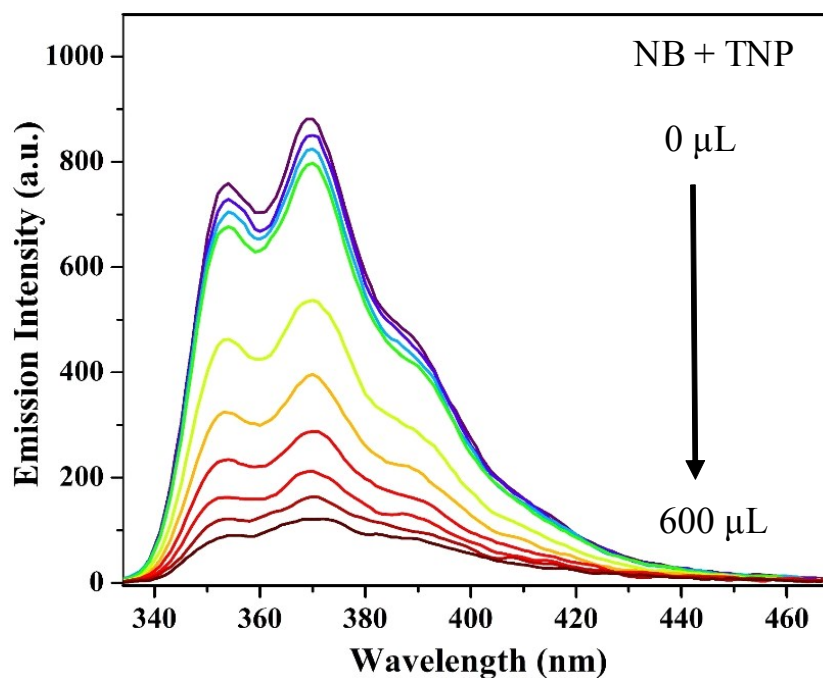
Figure S17. The emission spectra of Zn-CP dispersion upon incremental addition of NB solution (300 µL, 1mM) followed by the addition of TNP solution (300 µL, 1mM) (λ_{ex} = 325 nm).
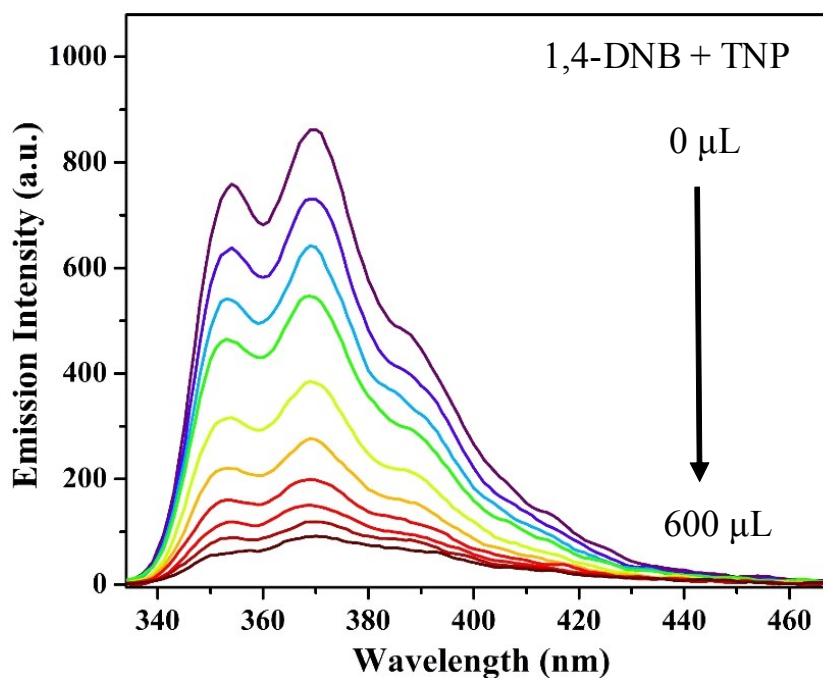
Figure S18. The emission spectra of Zn-CP dispersion upon incremental addition of 1,4-DNB solution (300 µL, 1mM) followed by the addition of TNP solution (300 µL, 1mM) (λ_{ex} = 325 nm).
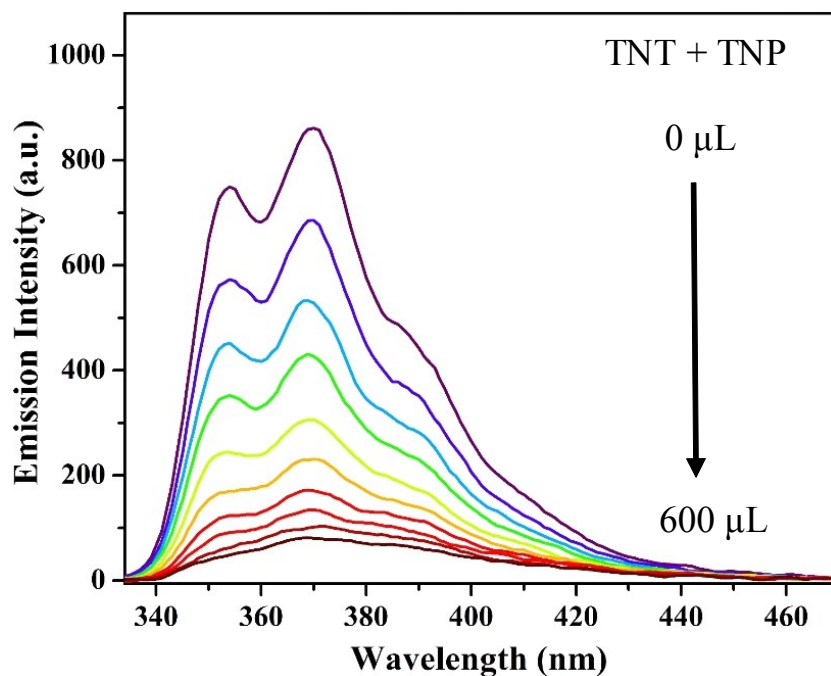
Figure S19. The emission spectra of Zn-CP dispersion upon incremental addition of TNT solution (300 µL, 1mM) followed by the addition of TNP solution (300 µL, 1mM) (λ_{ex} = 325 nm).
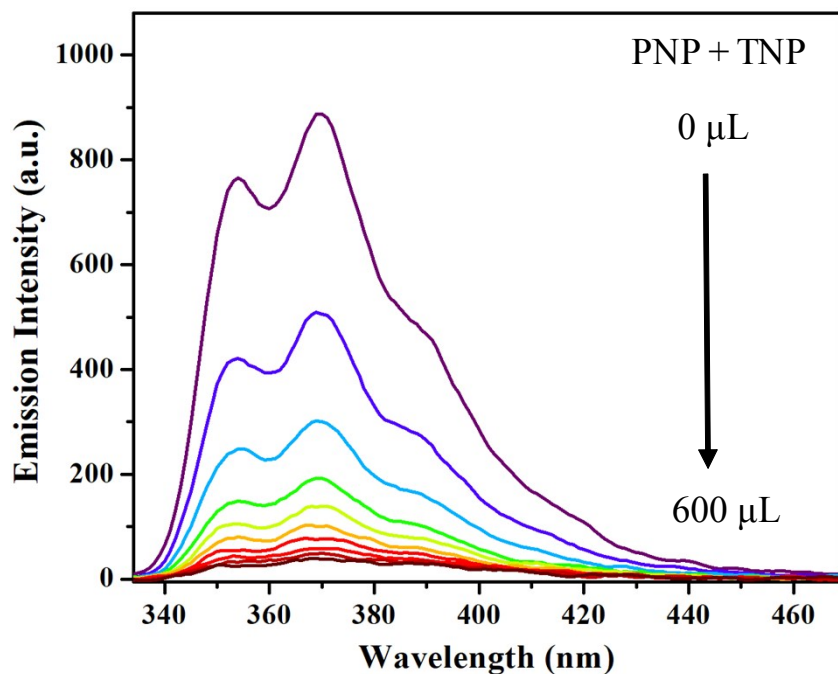
Figure S20. The emission spectra of Zn-CP dispersion upon incremental addition of PNP solution (300 µL, 1mM) followed by the addition of TNP solution (300 µL, 1mM) (λ_{ex} = 325 nm).
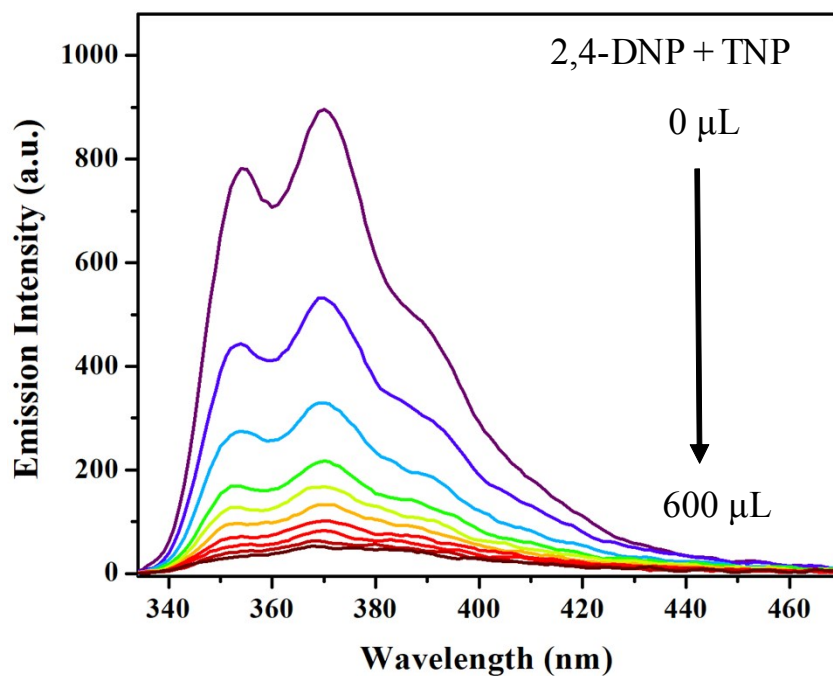
Figure S21. The emission spectra of Zn-CP dispersion upon incremental addition of 2,4-DNP solution (300 μL, 1mM) followed by the addition of TNP solution (300 μL, 1mM) (λ_{ex} = 325 nm).
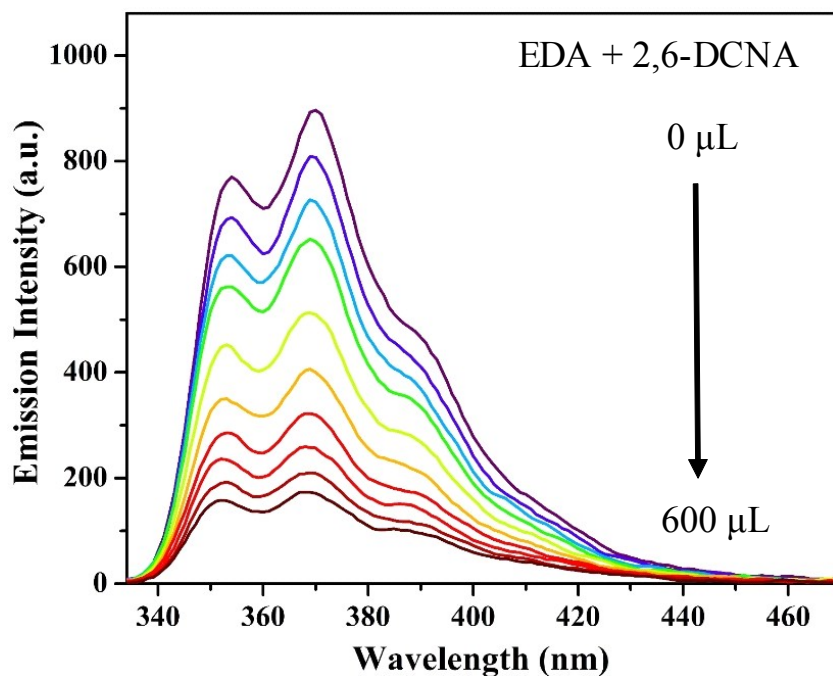
Figure S22. The emission spectra of Zn-CP dispersion upon incremental addition of EDA solution (300 μL, 1mM) followed by the addition of 2,6-DCNA solution (300 μL, 1mM) (λ_{ex} = 325 nm).
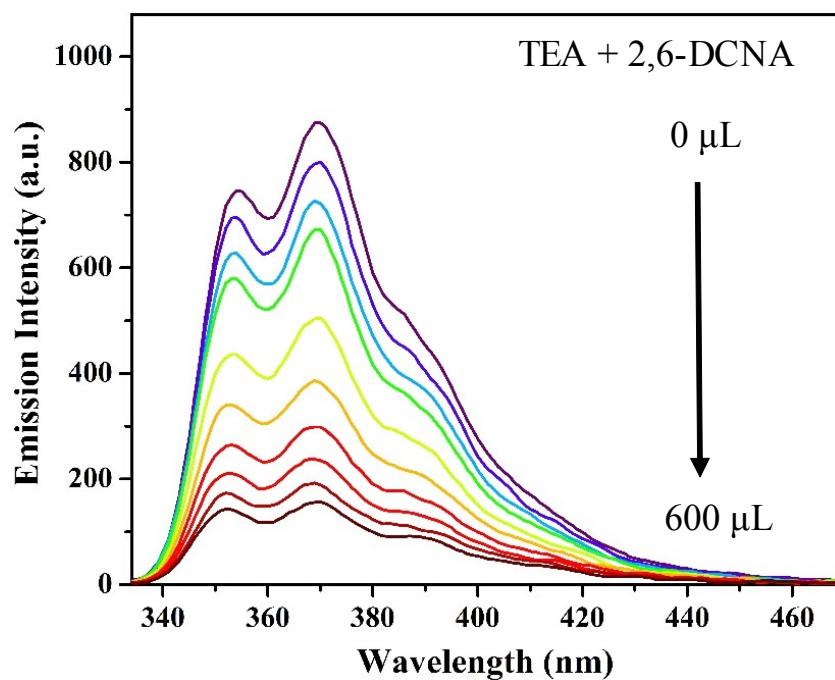
Figure S23. The emission spectra of Zn-CP dispersion upon incremental addition of TEA solution (300 µL, 1mM) followed by the addition of 2,6-DCNA solution (300 µL, 1mM) (λ_{ex} = 325 nm).
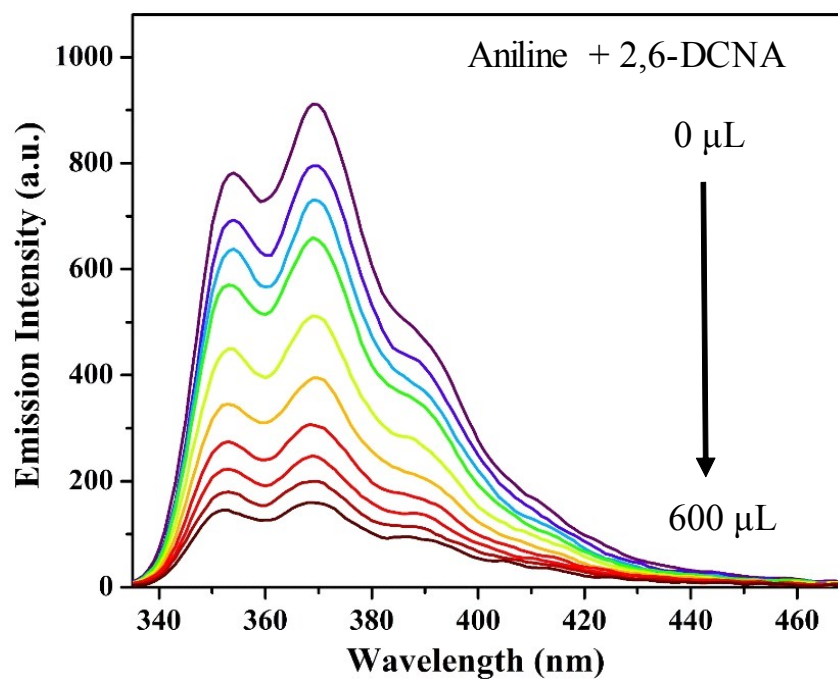
Figure S24. The emission spectra of Zn-CP dispersion upon incremental addition of aniline solution (300 µL, 1mM) followed by the addition of 2,6-DCNA solution (300 µL, 1mM) (λ_{ex} = 325 nm).
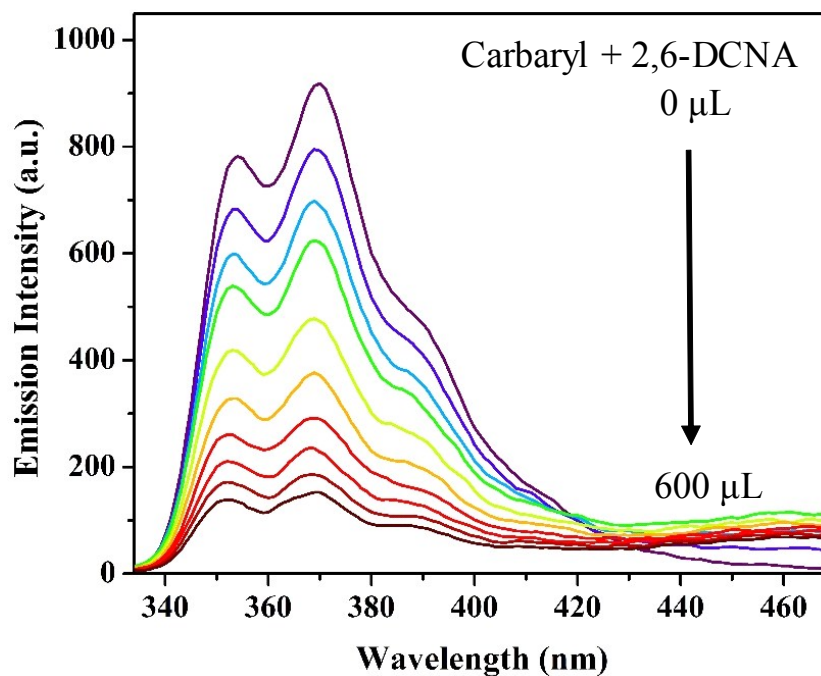
Figure S25. The emission spectra of Zn-CP dispersion upon incremental addition of carbaryl solution (300 μL, 1mM) followed by the addition of 2,6-DCNA solution (300 μL, 1mM) (λ_{ex} = 325 nm).
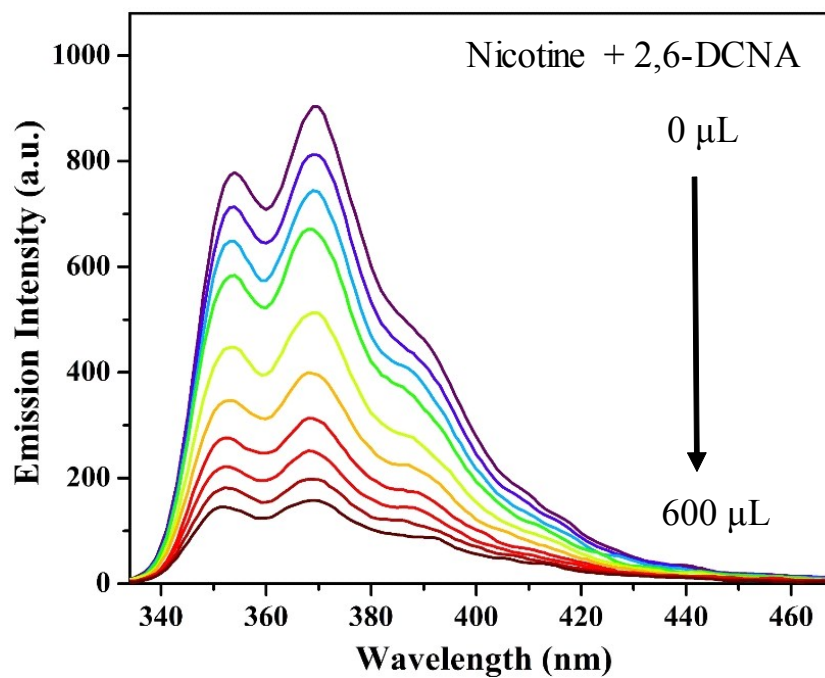
Figure S26. The emission spectra of Zn-CP dispersion upon incremental addition of nicotine solution (300 μL, 1mM) followed by the addition of 2,6-DCNA solution (300 μL, 1mM) (λ_{ex} = 325 nm).
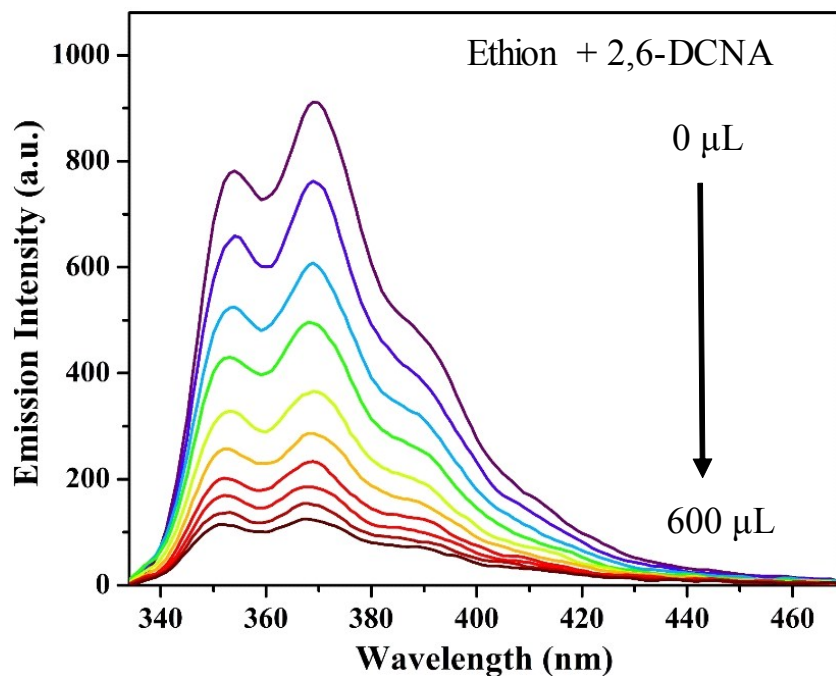
Figure S27. The emission spectra of Zn-CP dispersion upon incremental addition of ethion solution (300 µL, 1mM) followed by the addition of 2,6-DCNA solution (300 µL, 1mM) (λ_{ex} = 325 nm).
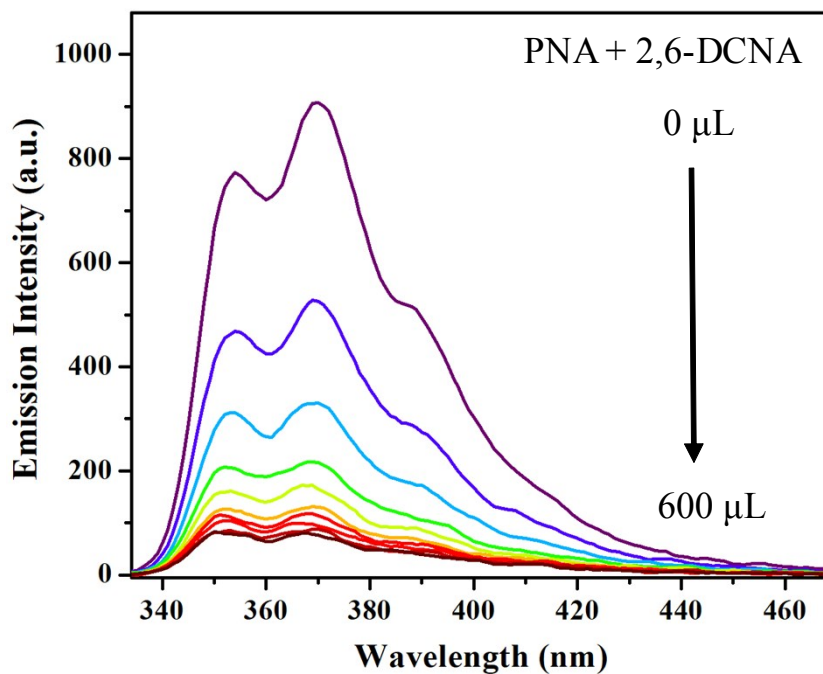
Figure S28. The emission spectra of Zn-CP dispersion upon incremental addition of PNA solution (300 µL, 1mM) followed by the addition of 2,6-DCNA solution (300 µL, 1mM) (λ_{ex} = 325 nm).

Determination the limit of detection (LOD) for TNP and 2,6-DCNA:

Detection limit was calculated on the basis of multiple number of fluorescence titration using the equation ($3\sigma/m$), where σ is the standard deviation of the blank solution, calculated from 10 blank measurements and m is the slope of the fluorescence intensity vs analyte concentration plot.[4]

The plot contains the following fitted data:

Equation	y = a + b*x		
Adj. R-Square	0.99684		
		Value	Standard Error
B	Intercept	8.00132	1.62501
B	Slope	26.09986	0.73495
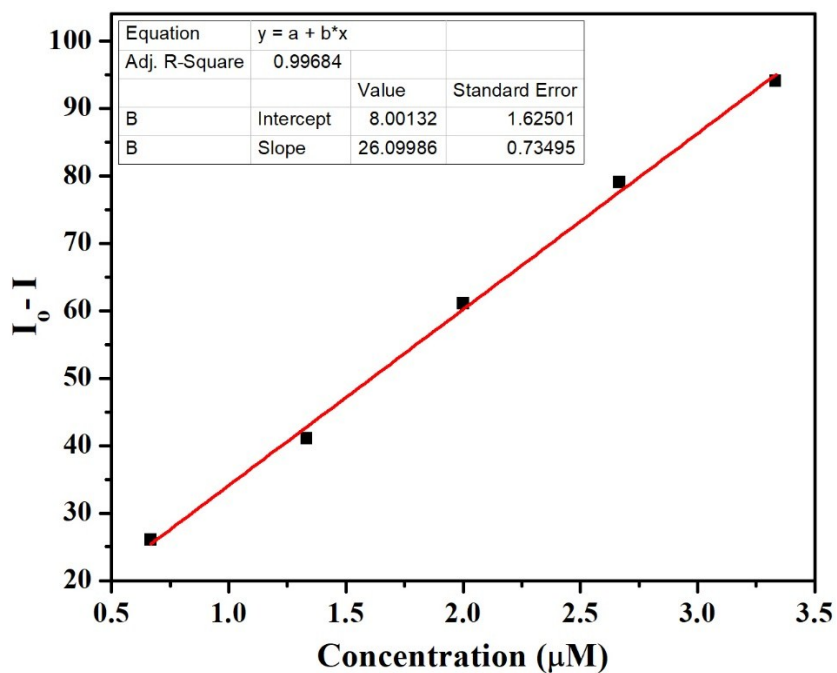
Figure S29. Plot of fluorescence intensity of Zn-CP in water as a function of concentration of TNP (λ_{ex} = 325 nm).
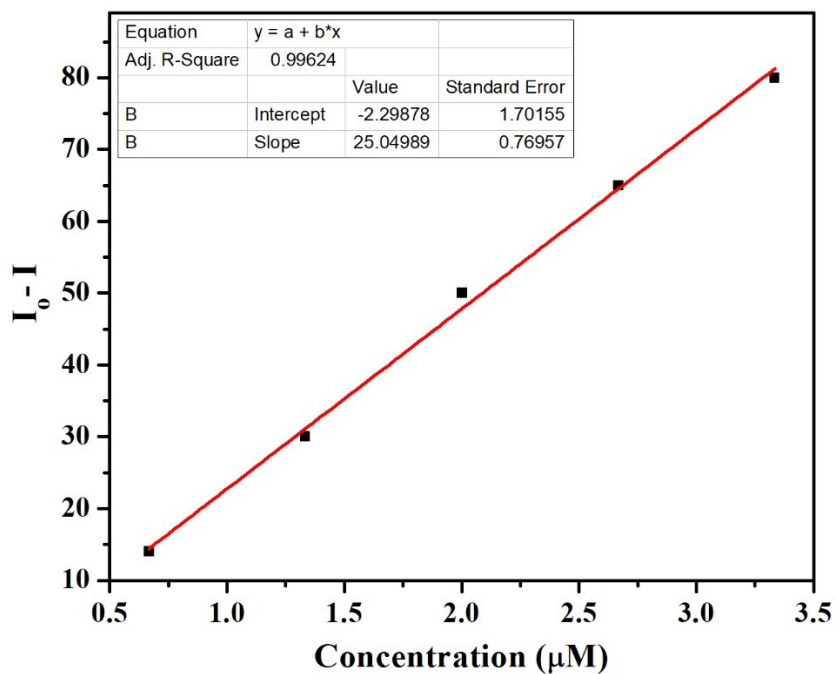
Figure S30. Plot of fluorescence intensity of Zn-CP in water as a function of concentration of 2,6-DCNA (λ_{ex} = 325 nm).

Standard deviation (σ)	0.5025
Detection limit of TNP	58 nM
Detection limit of 2,6-DCNA	60 nM
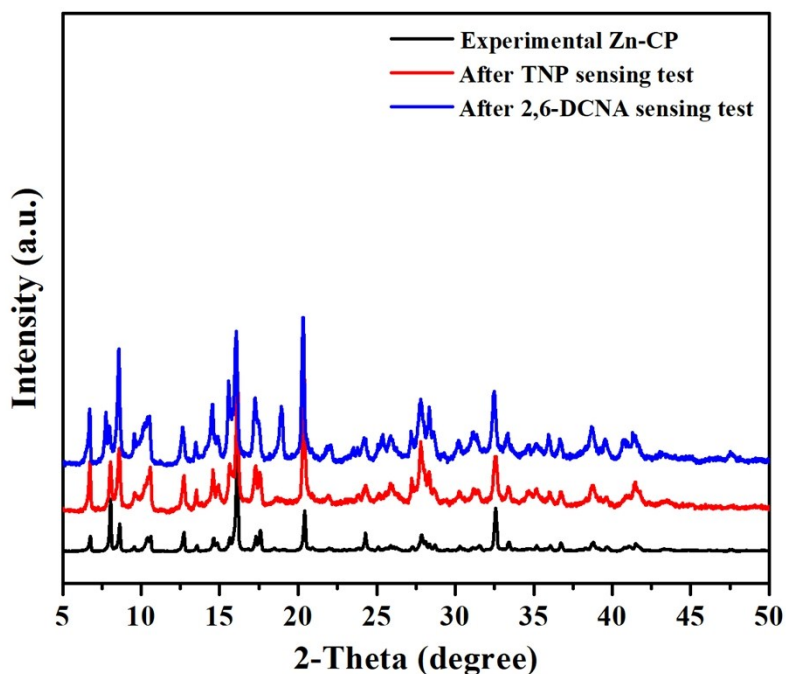
Figure S31. PXRD patterns of Zn-CP before and after the sensing test.

Recyclability test of Zn-CP:

The recyclability test of Zn-CP was performed with recovered material. The recovered material was collected after centrifugation followed by filtration, and finally washed two times with Water/EtOH solution.
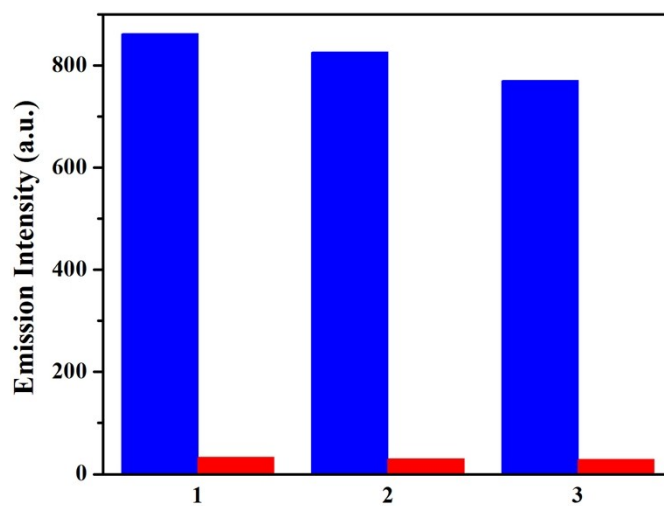
Figure S32. Recyclability plot of Zn-CP for three consecutive cycles in the presence of TNP solution [blue bars represent the initial emission intensity of Zn-CP and the red bars represent the emission intensity after the addition of TNP solution (600 μL, 1 mM)] (λ_{ex} = 325 nm).
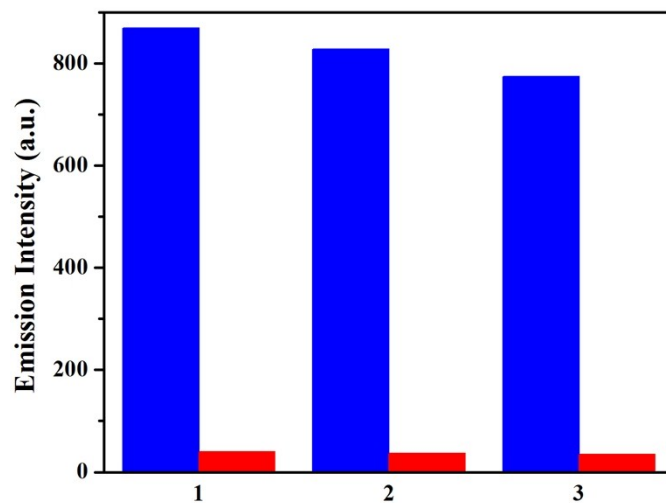
Figure S33. Recyclability plot of Zn-CP for three consecutive cycles in the presence of 2,6-DCNA solution [blue bars represent the initial emission intensity of Zn-CP and the red bars represent the emission intensity after the addition of 2,6-DCNA solution (600 μL, 1 mM)] (λ_{ex} = 325 nm).

Description of Theoretical Methods:

The electronic structure studies of a model Zn-CP and corresponding analytes were performed using density functional theory (DFT) as implemented in the Gaussian 09 suite of programs.[5] The structures of all isolated molecules and the hydrogen-bonded complexes with analytes were determined by full geometry optimization in the gas-phase using M06[6] functional (and B3PW91[7,8] in some cases for re-checking, Table S4) with the 6-31G** basis-set and subsequently frequency calculations were performed to ascertain the stationary points. Since hydrogen-bonding interaction is a non-covalent interaction, arising from electron-electron correlations, only advanced post Hartree-Fock methods like MP2, CCSD give results comparable to experiments, and common DFT methods based on LDA/GGA or even hybrid functionals like B3LYP are not adequate. It was later pointed out that the hybrid M06 functional combined with modest basis sets qualitatively reproduces the potential energy surfaces of higher level calculations for a number of hydrogen bonding and C-H$\cdots\pi$ cases.[9] In this case we use the results from calculations using M06 functional as it was previously shown to give best results for various non-covalent interactions.[9]

The optimized structure of Zn-CP is shown in Figure S34a. We have calculated the frontier molecular orbitals of the model Zn-CP and it is seen that the first four levels including HOMO is almost degenerate (see Figure S34b). These MOs are located on one of the four paddles of the paddle wheel motif containing Zn atoms in Zn-CP. We have also calculated the binding energies of few selected analytes (2,6 dichloro-4-nitroaniline, 2,4-Dinitrophenol and Trinitrophenol) to the model Zn-CP structure in gas-phase, according to the expression:

$E_{bind} = [E_{(Zn-CP)-analyte}] - [E_{Zn-CP} + E_{analyte}]$

The binding occurs due to hydrogen-bonding interactions between the imidazole moiety of Zn-CP and the nitro group of the nitroaromatics and it is calculated to be 11 kcal for 2,6 dichloro-4-nitroaniline while it is 7 and 6 kcal respectively for 2,4-Dinitrophenol and Trinitrophenol, thus the first one binds stronger. The optimized structures of the bound complex is shown in Figure 34c, d and e with the hydrogen-bonds marked in them.

In Figure 4, the relative HOMO and LUMO energy levels of all analytes are shown with respect to the HOMO and LUMO level of Zn-CP. It is seen that other than nicotine, for all the analytes,

the LUMO energy level is lower in energy compared to the LUMO energy of Zn-CP. So these unoccupied orbitals are suitably placed for transfer of electrons from the electron-rich Zn-CP framework to the analytes in case of excitation caused by photons. Our analysis of frontier molecular orbitals for the Zn-CP bound analytes (2,6 dichloro-4-nitroaniline, 2,4-Dinitrophenol and Trinitrophenol) shown in Figure S35, indeed reveal that the LUMO in these bound complexes are localized on the analytes, whereas the HOMO is localized on Zn-CP. So during excitation, an electron from Zn-CP bound HOMO is first transferred to some higher lying Zn-CP bound unoccupied orbital, which readily relaxes to the lowest unoccupied orbital based on the analyte resulting in fluorescence quenching.
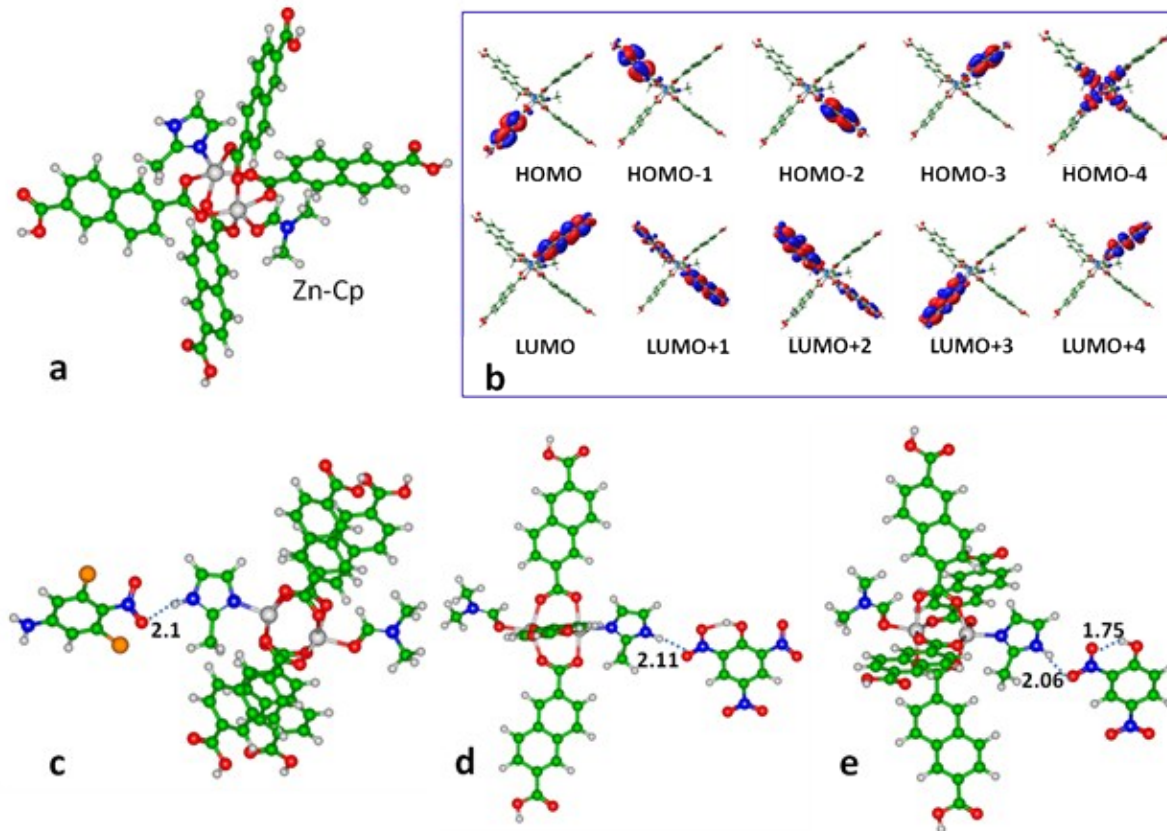
Figure S34. (a) The model structure of Zn-CP taken for theoretical DFT studies. It is chosen such that it reflects the portions important for the chemistry between the Zn-CP and the analytes. (b) The calculated frontier molecular orbital of Zn-CP. (c) The optimized structure of 2,6 dichloro-4-nitroaniline bound Zn-CP. (d) The optimized structure of Trinitrophenol bound Zn-CP. (e) The optimized structure of 2,4-Dinitrophenol bound to Zn-CP.
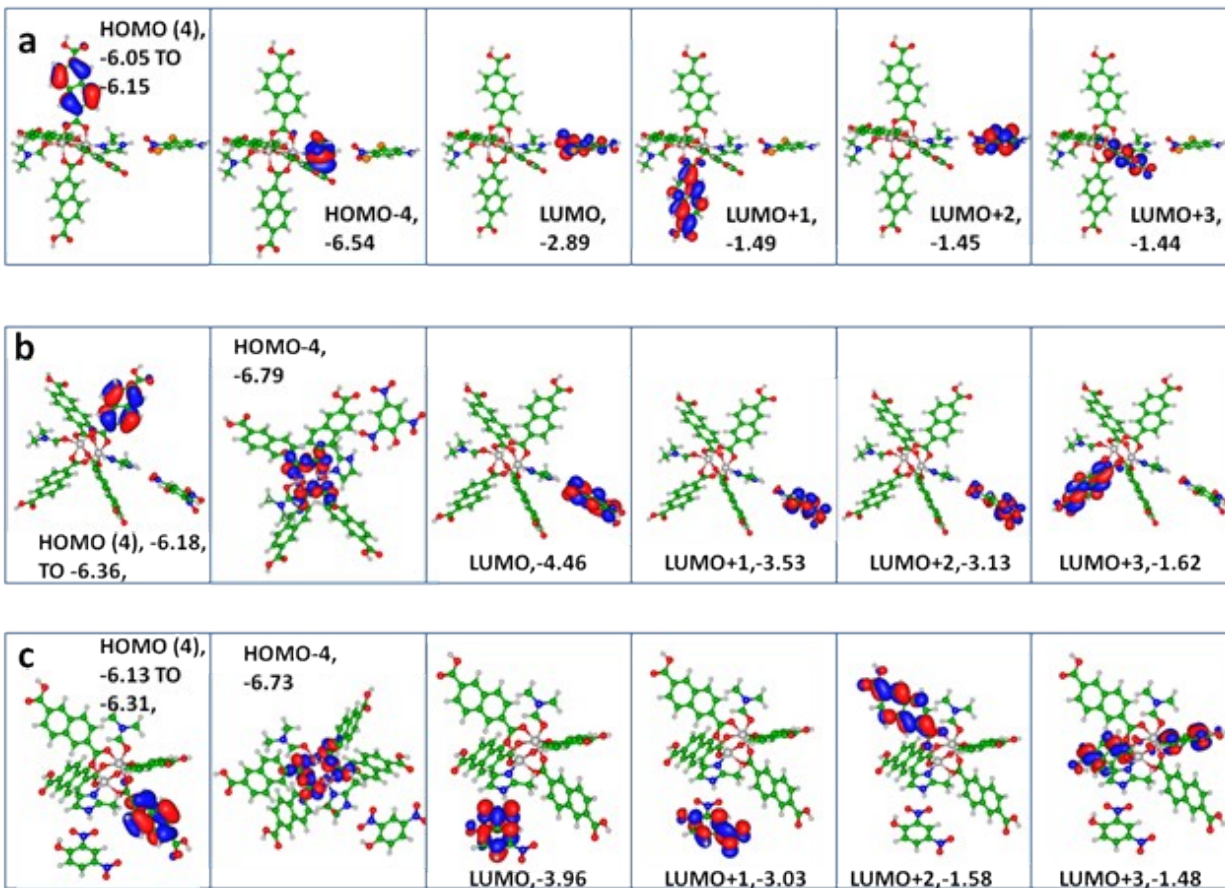
Figure S35. Frontier molecular orbitals of Zn-CP bound to (a) 2,6 dichloro-4-nitroaniline (b) Trinitrophenol and (c) 2,4-Dinitrophenol. The HOMO and LUMO are shown along with other inner orbitals marked as HOMO-n and LUMO+n, where n is the number by which it differs from either HOMO or LUMO. Thus, HOMO-n have energies more negative than HOMO, whereas LUMO+n have energies higher than LUMO.

Table S4. Theoretically calculated values of HOMO, LUMO and HOMO-LUMO gaps in eV for Zn-CP and few selected analytes using two different DFT functionals M06 and B3PW91.

Molecules/Complex studied	HOMO, LUMO, HOMO-LUMO Gap (eV), M06 /6-31G**	HOMO, LUMO, HOMO-LUMO Gap (eV), B3PW91 /6-31G**
Trinitrophenol	-8.62,-3.72, 4.90	-8.31,-3.97, 4.34
2,6 Dichloro 4 Nitro Aniline	-6.85, -1.90, 4.95	-6.57, -2.10, 4.47
2,4 Di nitrophenol	-7.98, -3.12, 4.86	-7.71, -3.38, 4.33
Zn-CP	-6.19, -1.65 , 4.54	-6.01, -1.85, 4.16
Zn-CP + Trinitrophenol	-6.20, -4.46,1.74	-6.02, -4.67, 1.35
Zn-CP + 2,6 dichloro 4 nitroaniline	-6.04, -2.89 ,3.15	-5.89, -3.10, 2.78
Zn-CP + 2,4 Di nitro phenol	-6.13, -3.97, 2.16	-5.96, -4.18, 1.78
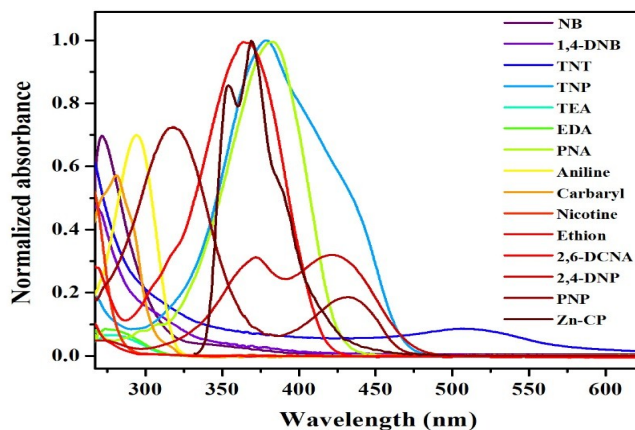
Figure S36. Spectral overlap between the normalized absorption spectra of the analytes and the normalized emission spectra of Zn-CP.

References:

1. CrysAlisPro Program, version 171.37.33c, Agilent Technologies, Oxford, 2012.

2. G. M. Sheldrick, *Acta Crystallogr*., 2008, **A64**, 112–122.

3. O. V. Dolomanov, L. J. Bourhis, R. J. Gildea, J. A. K. Howard and H. Puschmann, *J. Appl. Crystallogr.,* 2009, **42**, 339– 341.

4. G. L.; Long, J. D. Winefordner, Limit of detection. A closer look at the IUPAC definition. *Anal. Chem.* 1983**, 55** , 712A-724A.

5. Gaussian 09, Revision C.01, M. J. Frisch, G. W. Trucks, H. B. Schlegel, G. E. Scuseria, M. A. Robb, J. R. Cheeseman, G. Scalmani, V. Barone, B. Mennucci, G. A. Petersson, H. Nakatsuji, M. Caricato, X. Li, H. P. Hratchian, A. F. Izmaylov, J. Bloino, G. Zheng, J. L. Sonnenberg, M. Hada, M. Ehara, K. Toyota, R. Fukuda, J. Hasegawa, M. Ishida, T. Nakajima, Y. Honda, O. Kitao, H. Nakai, T. Vreven, J. A. Montgomery, Jr. J. E. Peralta, F. Ogliaro, M. Bearpark, J. J. Heyd, E. Brothers, K. N. Kudin, V. N. Staroverov, T. Keith, R. Kobayashi, J. Normand, K. Raghavachari, A. Rendell, J. C. Burant, S. S. Iyengar, J. Tomasi, M. Cossi, N. Rega, J. M. Millam, M. Klene, J. E. Knox, J. B. Cross, V. Bakken, C. Adamo, J. Jaramillo, R. Gomperts, R. E. Stratmann,O. Yazyev, A. J. Austin, R. Cammi, C. Pomelli, J. W. Ochterski, R. L. Martin, K. Morokuma, V. G. Zakrzewski, G. A. Voth, P. Salvador, J. J. Dannenberg, S. Dapprich, A. D. Daniels,O. Farkas, J. B. Foresman, J. V. Ortiz, J. Cioslowski, and D. J. Fox, Gaussian, Inc., Wallingford CT, 2010.

6. Y. Zhao, D. G. Truhlar, *Theor. Chem. Acc*., 2008, **120**, 215-41.

7. J. P. Perdew, J. A. Chevary, S. H. Vosko, K. A. Jackson, M. R. Pederson, D. J. Singh and C. Fiolhais, *Phy. Rev. B,* 1992, **46**, 6671.

8. J. P. Perdew, K. Burke and Y. Wang, *Phy. Rev. B*, 1996, **54**, 16533.

9. Thanthiriwatte, K. S.; Hohenstein, E. G.; Burns, L. A.; Sherrill, C. D., "Assessment of the Performance of DFT and DFT-D Methods for Describing Distance Dependence of Hydrogen-Bonded Interactions," *J. Chem. Theory Comput.*, 2011, **7**, 88-96.